



Droplet dynamics in a polymer electrolyte fuel cell gas flow channel: Forces, Deformation and detachment. II: Comparisons of analytical solution with numerical and experimental results

Sung Chan Cho^a, Yun Wang^{a,*}, Ken S. Chen^b

^a Renewable Energy Resources Lab (RERL) and National Fuel Cell Research Center, Department of Mechanical and Aerospace Engineering, The University of California, Irvine, CA 92697-3975, USA

^b Sandia National Laboratories, 7011 East Ave, Livermore, CA 94580, USA

ARTICLE INFO

Article history:

Received 11 February 2012

Received in revised form 10 March 2012

Accepted 12 March 2012

Available online xxx

Keywords:

Droplet
Detachment
Deformation
PEFC
Experiment
VOF

ABSTRACT

Proper water management (sufficient membrane hydration and effective liquid-water removal from catalyst layers, gas-diffusion layers, and channels) is key to achieving and maintaining the high performance of polymer electrolyte fuel cells (PEFCs). Specifically, liquid droplet formation and removal is an important issue in water management for PEFCs. In the first part of this series, explicit analytical solutions were derived by approximating the droplet shape as spherical and the Navier–Stokes equations were numerically solved to compute the forces over a droplet. In this second part of the series, results from numerical simulation using the Volume-of-Fluid (VOF) method and experiments are reported and they are compared with the analytical solutions derived previously. More specifically, experimental visualization of droplet dynamics in a micro channel is carried out. A high resolution CCD camera is employed to capture the droplet shape-change and detachment. Extensive numerical simulations via VOF are also performed to investigate droplet dynamics. Reasonably good agreements between analytical solution and VOF numerical simulation and experiment are obtained.

© 2012 Elsevier B.V. All rights reserved.

1. Introduction

Proper water management (sufficient membrane hydration and effective liquid-water removal from catalyst layers, gas-diffusion layers, and channels) is key to achieving and maintaining the high performance of polymer electrolyte fuel cells (PEFCs). Specifically, liquid water removal from PEFC channels is an active and important area of research in PEFCs. Specifically, water droplet formation frequently occurs at the gas diffusion layer (GDL) surfaces in the gas flow channel of PEFCs [1–3]. One source of liquid water is from condensation: when the vapor partial pressure reaches the saturated one, excessive water in the vapor phase condenses to liquid water. The other is from liquid-water production directly by the electrochemical reaction in catalyst layers. Liquid water produced in the cathode catalyst layer can be absorbed into membrane and transported to anode side by diffusion or permeation. It can also be delivered to the cathode gas channel via the GDL. At the hydrophobic GDL interface, liquid can aggregate to form droplets and grow its volume until it is removed by the reactant

gas flow. Droplet formation can increase transport polarization, and consequently reduce cell performance.

Droplet dynamics in a micro/mini channel have been studied through simplified analysis, numerical simulation, and visualization experiments. Early studies on droplet dynamics for PEFC application mainly used optical visualization to examine droplet formation and removal. Yang et al. [4] placed a transparent window on a multi-channel PEFC, showing droplet formation and channel blocking. Wang et al. [5] showed experimental visualization of two-phase flow in multiple gas flow channels, indicating droplet formation. They also linked the two-phase flow to the pressure drop and further cell voltage oscillation when decreasing the stoichiometry to around 2.0. Chen et al. [6] conducted experiments on an operating PEFC with a transparent channel wall and was able to observe the formation and breakup/detachment of water droplets on the GDL surface. They also pioneered droplet instability/detachment visualization experiments using a specially designed visualization apparatus with transparent channel walls, and developed droplet-instability windows. Ma et al. [7] linked the droplets in channels to the pressure drop and use it for water removal diagnosis. Wang [8] indicated that droplets form and attach to the side wall of a channel. Theodorakakos et al. [9] used transparent PEFCs to study droplet detachment. Static and

* Corresponding author. Tel.: +1 949 824 6004; fax: +1 949 824 8585.
E-mail address: yunw@uci.edu (Y. Wang).

Nomenclature

A	area (m^2)
D/d	droplet diameter (m, mm)
D_H	hydraulic diameter (m)
F	force (N)
H	channel height (m)
\hat{i}	direction vector (-)
\hat{n}	normal vector (-)
p	pressure (pa)
R	local curvature (m)
RH	relative humidity (-)
S_m	mass source term ($\text{kg m}^{-3} \text{s}^{-1}$)
r	droplet radius (m)
\hat{t}	tangential vector (-)
u	velocity (m s^{-1})
W	channel width (m)
We_r	Weber number (-)

Greek letters

α	volume fraction (-)
γ	surface tension (N m^{-1})
θ	contact angle (rad, deg)
μ	viscosity ($\text{kg m}^{-1} \text{s}^{-1}$)
ρ	density (kg m^{-3})

dynamic contact angles were measured and compared with VOF (Volume of Fluid) simulation results. The VOF has been regarded as a useful numerical tool to study the droplet dynamics thanks to its capability of tracking liquid–gas interface. Zhu et al. [10] used VOF for parametric study on the impact of channel dimension on droplet detachment velocity. Bazylak et al. [11] studied droplet emergence and detachment through VOF simulation and ex situ experiment. Hao and Cheng [12] analytically predicted dynamic contact angle and droplet velocity in a micro channel. The results are compared to LBM (Lattice Boltzmann Method) simulation. An explicit analytical model to predict the droplet instability in the viscous-force-dominating flow regime (i.e., Reynolds number is vanishingly small) was proposed by Chen et al. [6] using the force balance approach. As mentioned earlier, visualization experiments were also conducted to generate data for comparison with model prediction. Kumbur et al. [13] proposed similar approach along with experimental work. More recently, Chen [18] presented an explicit analytical model for predicting droplet-detachment velocity in the inertia-dominating flow regime.

Though many studies have been proposed to understand droplet dynamics, explicit analytical models that can be employed as tools for PEFC design and optimization are still in great need and their comparisons with experimental data are lacking. In the first part of this paper series, analytical solutions for predicting droplet deformation and detachment were derived by approximating the droplet shape as spherical. The Weber number and Reynolds number are linked to droplet shape-change and removal through analytical solutions. In the present work (which is the second part), experiments and VOF numerical simulation (without approximating the droplet shape as spherical) on droplet deformation and detachment were conducted and the results were compared with the analytical solutions. We hope the discussion of forces, deformation, and detachment will provide a comprehensive picture of droplet dynamics over GDL surfaces. Again the results are beneficial to the fundamental understanding of droplet formation and detachment at GDL surface, which is of vital importance to flow field design and water management for

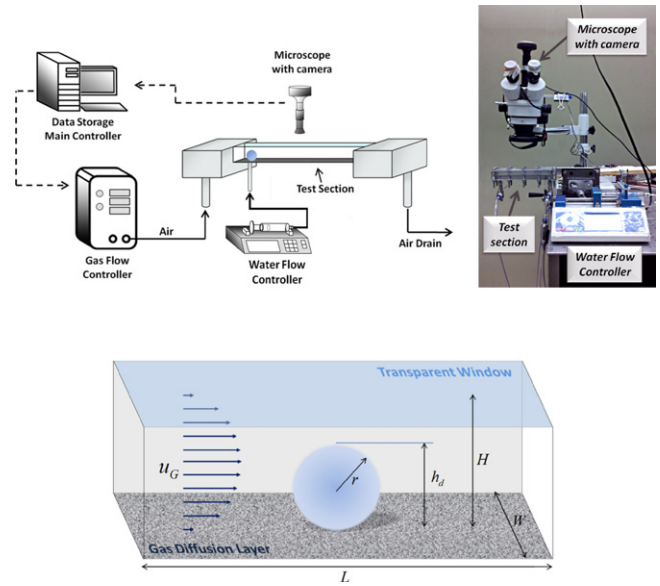


Fig. 1. Schematic and picture of experimental setting (top); and schematic of a droplet in a gas flow channel (bottom).

PEFCs. For example, the analytical solutions contain parameters such as the channel dimension, surface tension, and detachment velocity, therefore they can be used to optimize flow channels and droplet removal strategy. Further, droplet dynamics over GDL surfaces is one major area of research in channel two-phase flow. There are other areas such as liquid flow over the hydrophilic channel sidewall and droplet removal when it reaches the sidewalls. It is also important to investigate all the issues by considering the entire channel due to the inherent connection between them. This will allow the material nature of the flow field as a whole to be accounted for in studying channel two-phase flow.

2. Analytical solutions

In the first part [14], the drag coefficient of a droplet in a micro channel as a function of the Reynolds number is generalized using:

$$C_D = a \times Re_H^b \quad (1)$$

where $a = 46.247 \times (D/H)^{0.1757}$ and $b = 0.2158 \times (D/H) - 0.6384$ in the fully developed region for the channel considered. With the above generalized formula, the detachment velocity in terms of the Weber number ($We_r \equiv \rho u^2 R_0 / \gamma$) can be expressed by:

$$We_r = \left[\frac{4\pi \sin^2 \theta_s \sin(1/2)(\theta_a - \theta_r)}{a (\theta_s - \sin \theta_s \cos \theta_s)} \right] Re_H^{-b} \quad (2)$$

Droplet deformation due to its obstruction can be evaluated by the Young–Laplace equation and Bernoulli's equation, which is quantified by the change of local curvature radius:

$$\frac{dR}{R} = \frac{We_r}{4} \left(1 - \frac{R_0^2}{A_C} (\theta_s - \cos \theta_s \sin \theta_s) \right)^2 \quad (3)$$

where R , R_0 and A_C are radius of local curvature, initial radius of droplet and cross sectional area of channel, respectively. Details of the analytical model can be found in the first part of this paper series [14].

Table 1
List of experiment cases.

Case No.	GDL	Channel cross section dimension (mm ²)	Contact angle	D_{drop}/D_H	Air flow velocity (m s ⁻¹)	Flow condition
1	Carbon paper (wet proof 30%)	1.6 × 1.0	128°	0.90	0.0–5.21	Fully developed
2	PTFE tape	1.6 × 1.0	115°	0.89	0.0–5.21	Fully developed
3	Carbon paper (wet proof 30%)	1.6 × 1.0	128°	0.69–1.01	0.0–8.75	Entrance length
4	Carbon paper (wet proof 30%)	1.6 × 1.0	128°	0.69–0.98	0.0–8.75	Fully developed

3. Experimental

Fig. 1 shows the experimental setup that was specially designed, fabricated and employed to study droplet dynamics in micro/mini channels. The gas flow channels were fabricated within both Aluminum and plastic thin plates, and both were used in experiment to ensure independence of the experimental data on channel wall materials. The channel has a cross-sectional dimension of 1.0 mm × 1.6 mm with length of 4.0 cm. The GDL material is the Toray carbon paper with 30% PTFE loading. A transparent plate was placed on the channel plate to provide optical window. A CCD camera was mounted over a microscope for visualizing droplet dynamics. The base plate was fabricated by CNC machining on Aluminum plates where air and water injection fittings were mounted. The hydrophobic carbon paper is placed on the base plate and clamped by the channel and the top transparent plates. Liquid droplet is generated by supplying water from the base plate via a small hole through the carbon paper. Water permeates the porous layer and forms a droplet on the GDL surface. Since the contact angle of hydrophobic materials are 104–128°, the droplet diameter can reach over channel height (1 mm) without touching the top surface. Once a droplet is formed in a static flow, the diameter of droplet is measured and gas velocity is increased gradually by 0.1 m s⁻¹ until the droplet is removed from the GDL surface. In real fuel cell operation, however, liquid water is added to form a droplet in air flow environment till its detachment. This likely makes no difference in terms of the forces, deformation and detachment of droplets because it is apparent that the physical presence of liquid droplet is the major cause. Further, the present method allows us to precisely measure the droplet size because it remains perfect spherical shape. When there is air flow, the droplet shape can change, making it difficult to measure the droplet dimension. As stated before, the water of droplets may come from vapor condensation in supersaturated gas or liquid transport through GDLs. Because of low temperature, condensation occurring at droplet surface is negligible, therefore it is the latter source that is primarily considered in the experiment. However, the sources of water have little effect on the forces, deformation, and detachment of droplets because they are primarily determined by the physical presence of liquid droplets. Similar

strategy is also used in Ref. [6]. The water injection hole was drilled on the base plate about 3.75 cm away from the channel manifold, i.e. the flow near the droplet site is in the fully developed condition. By placing honeycomb (porous material) in the upstream gas channel near the droplet inlet hole, the flow field at the droplet site can be modified, i.e. the droplet is subject to air flow in the entrance region. The entire test section was placed on the pneumatic isolated table to eliminate any noises from external disturbance. Air flow rate is controlled by the mass flow controller in a fuel cell test station with 100% relative humidity. Details of the experimental cases are listed in Table 1. Droplets on the surfaces of the two materials are shown in Fig. 2. Note that the experimental set up is similar to that used by Adroher and Wang [15], which was designed to study two-phase flow pattern and pressure drop.

4. Numerical simulation: Volume of Fluid (VOF) method

A three-dimensional model, based on the VOF method [16] (which is one of the most popular numerical techniques to trace the interface of two phases and study multiphase flows), was developed and used to simulate the water-droplet dynamics (deformation, detachment). With this method, the equations that govern mass and momentum conservations are solved in conjunction with the volume fraction equation. The former can be expressed as:

$$\frac{\partial}{\partial t} \rho + \nabla \cdot (\rho \vec{u}) = S_m \quad (4)$$

$$\frac{\partial}{\partial t} (\rho \vec{u}) + \nabla \cdot (\rho \vec{u} \vec{u}) = -\nabla p + \nabla \cdot (\mu (\nabla \vec{u} + \nabla \vec{u}^T)) + \rho \vec{g} + \vec{F}_{Vol} \quad (5)$$

The momentum source term \vec{F}_{Vol} on the right hand side of the equation takes into account the surface tension γ , surface curvature k_k and gradient of the volume fraction $\nabla \alpha_k$. The volume fraction α_k is defined as the portion of a computational cell filled with k th phase of fluid. In this study, the primary fluid is set as air and the secondary fluid is liquid water. Thus, any computational cell filled with only air has the value of zero for α_{water} . For the computational cell filled with liquid water, α_{water} becomes unity. A value between zero and unity means the cell contains the two-phase interface. To

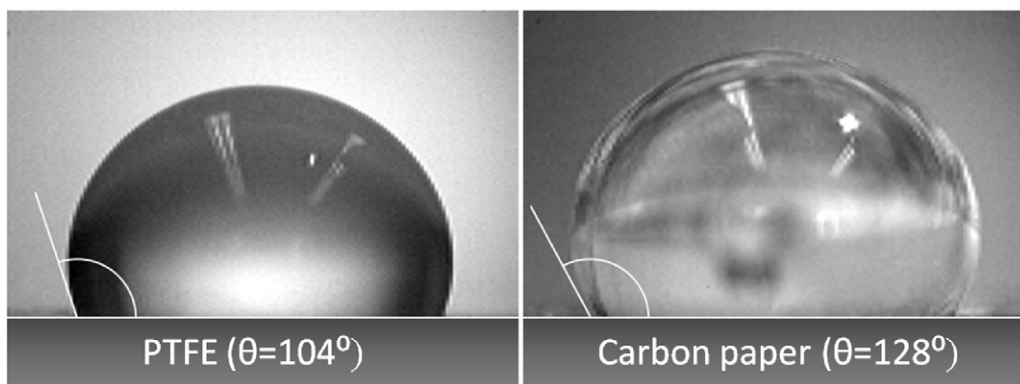


Fig. 2. The contact angles of two hydrophobic materials.

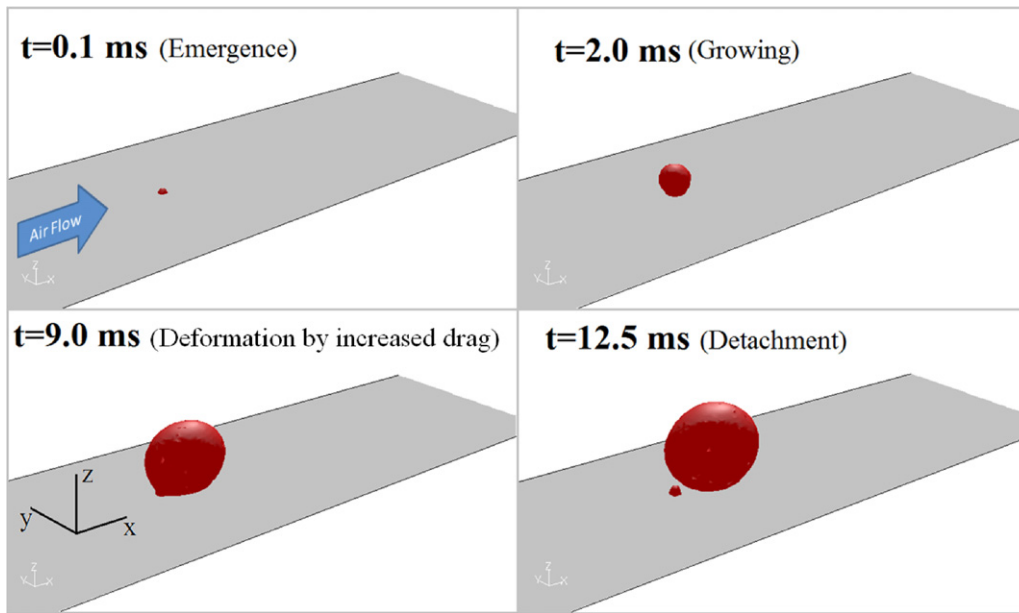


Fig. 3. Water droplet dynamics simulated by the 3D VOF (channel height = 1.0 mm, $U_G = 2.0 \text{ m s}^{-1}$, $\theta = 150^\circ$).

satisfy the continuum theory of fluid, the summation of α in a cell satisfies:

$$\alpha_{water} + \alpha_{air} = 1 \quad (6)$$

The volume fraction is governed by the following volume fraction equation:

$$\frac{\partial}{\partial t}(\alpha_{air} \rho_{air}) + \nabla \cdot (\alpha_{air} \rho_{air} \vec{u}_{air}) = 0 \quad (7)$$

This volume fraction conservation equation is correlated with the mass and momentum equations through the volumetric force term (\vec{F}_{Vol}) and solved every iteration step for all computational cells. The properties of fluids at the interface between gas and liquid are weight-averaged by the volume fraction in the cell, for example:

$$\rho = \rho_{air} + \alpha_{water}(\rho_{water} - \rho_{air}) \quad (8)$$

Through this averaging, fluids in interface can be regarded as single phase and only one set of governing equations needs to be solved in the interface region. For the local curvature of interface, the Young–Laplace equation can be utilized considering two radii in the orthogonal direction (R_1 & R_2):

$$\Delta p = \gamma \left(\frac{1}{R_1} + \frac{1}{R_2} \right) \quad (9)$$

The surface tension force is related to the momentum source by using the CSF (continuum surface force) model [17], in which the force can be expressed as:

$$\vec{F}_{Vol} = \gamma \frac{\rho k_k \nabla \alpha_k}{(1/2)(\rho_k + \rho_j)} \quad (10)$$

where, $k_k = \nabla \cdot \hat{n}$, $n = \nabla \alpha_k$, and $\hat{n} = n/|n|$.

At the contact line on the GDL surface, droplet and air, the surface normal \hat{n} is determined by the static contact angle θ_s :

$$\hat{n} = \hat{n}_w \cos \theta_s + \hat{t}_w \sin \theta_s \quad (11)$$

where \hat{n}_w and \hat{t}_w are the normal and tangential vectors, respectively, to the wall surface. Based on this surface normal, the local curvature near the wall boundary and surface tension force are determined in turn. In the present work, about 576,000 hexahedral computational cells were used in the VOF simulation. For the

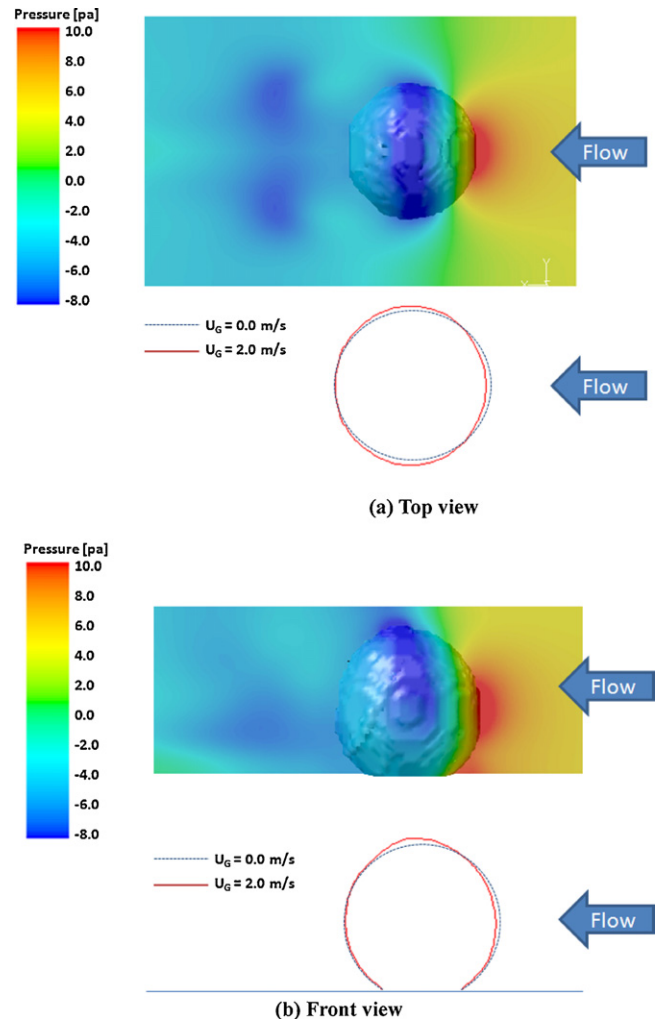


Fig. 4. Air pressure distribution near a water droplet (top) and droplet shape change (bottom).

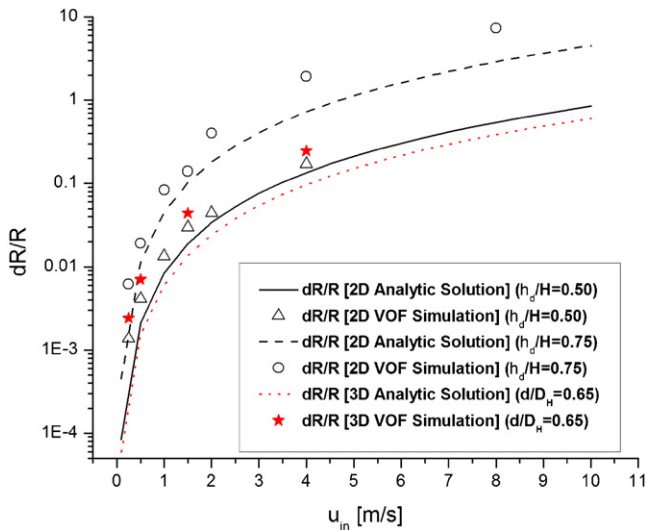


Fig. 5. Comparison of analytical solution with the VOF results.

pressure & velocity coupling, the SIMPLE method is used, and the governing equations are discretized through PRESTO! using the second order upwind method. In this work, commercial CFD (Computational Fluid Dynamics) solver Fluent (version 6.3.26) was used to carry out the VOF numerical simulation.

5. Results and discussion

5.1. Droplet shape change

Fig. 3 shows an example of the water droplet dynamics simulated using the 3D VOF method. A droplet forms at the site of the hole by liquid injection. At low velocity, the wall adhesion is sufficient to keep the droplet still on the surface. As the gas flow rate increases, the drag force increases rapidly [14], which eventually overcomes the adhesion force and removes the droplet from the surface. In the first part of this paper series [14], the droplet shape change caused by the pressure difference is quantified by an analytical solution derived by approximating the droplet shape as spherical. Fig. 4 shows the gas pressure contours predicted by the VOF simulation, indicating the gas phase pressure can vary substantially due to the obstruction of the droplet. At the stagnation point in the front of the droplet, the local gas pressure is increased, while

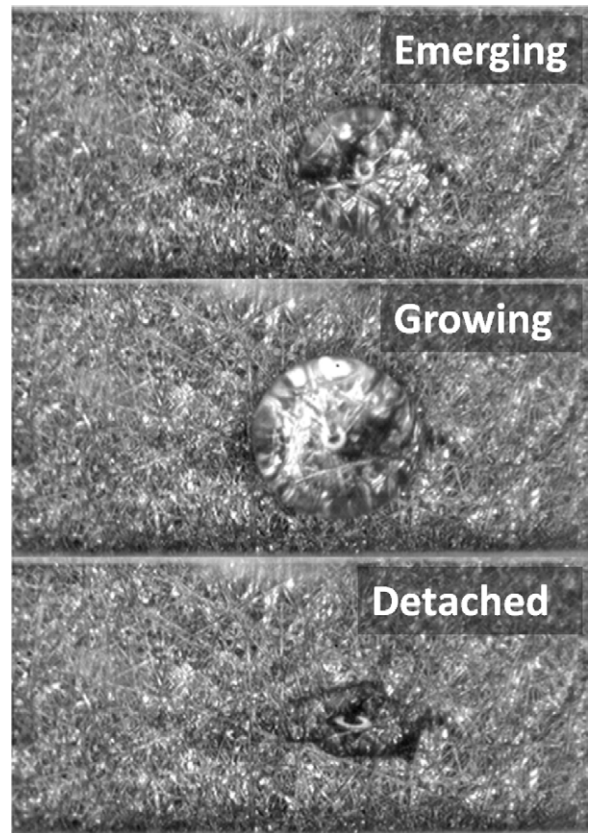


Fig. 6. Visualization of droplet dynamics in a micro gas flow channel.

at the location where the cross sectional area for gas flow decreases to the minimum and the local gas velocity increases to maximum, local pressure becomes low. It can be seen that the droplet shape is changed and slightly deviates from the spherical shape: at the lower gas pressure site the surface curvature is larger to balance the pressure difference between gas and liquid; at the higher gas pressure site the liquid withdraws resulting in a smaller curvature.

The droplet deformation caused by the pressure variation can be directly calculated through the liquid–gas interface shape predicted by the VOF method, and the result from a case study is plotted in Fig. 5 together with that predicted by the analytical solution. For both 2D and 3D simulation, the VOF results show slightly larger

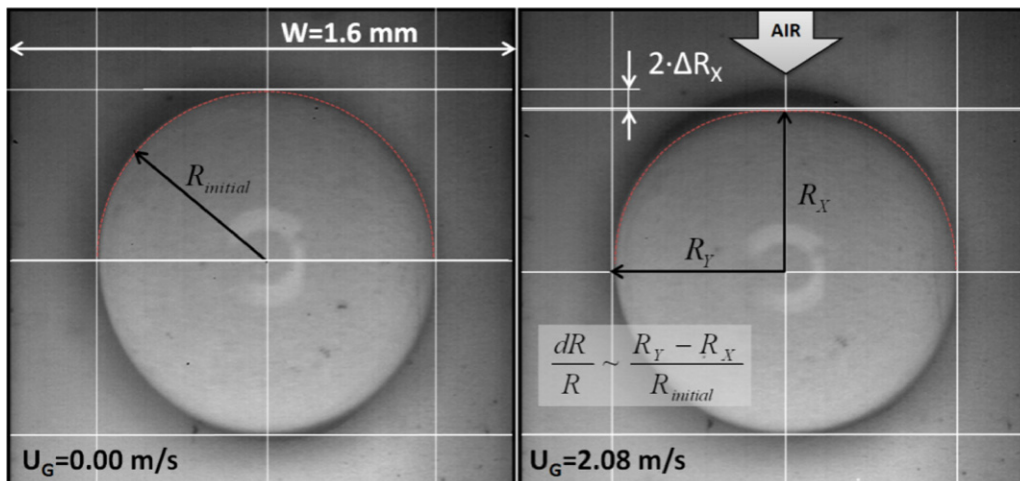


Fig. 7. Experimental observation of droplet shape change on hydrophobic GDL surface, PTFE (case 2) ($\theta_s = 115^\circ$).

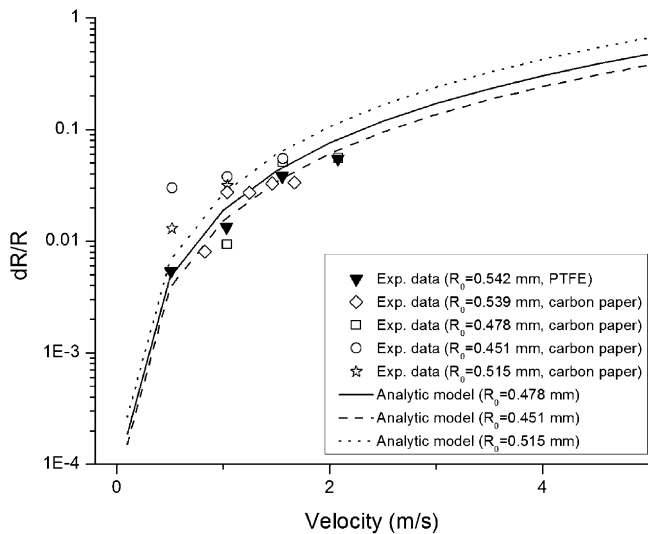


Fig. 8. Comparison of droplet deformation between the analytical solution and experimental data.

deformation but the trends are in good agreement. The discrepancy may be due to that the average velocity is used in the analytical solution whereas there is a local velocity variation in the VOF numerical simulation.

Experimentally, the droplet shape-change was captured using a high-resolution camera. GDL surfaces were examined in this work, the carbon paper ($\theta = 128^\circ$) and PTFE surface ($\theta = 104^\circ$), see Fig. 2. Fig. 6 displays the visualization of droplet emerging, growth, and detachment on a carbon paper surface whereas Fig. 7 shows the visualization of droplet deformation on the PTFE surface. In Fig. 6, the droplet was introduced into the channel where exists air flow, similar to what happens in PEFC channels. Fig. 8 compares the experimental data with the analytical solution. Due to the hysteresis of the contact angle, it was difficult to determine the droplet front line (or upstream front) optically at high velocity in experiment; consequently, we focused on the regime with velocity less than 2.0 m s^{-1} . It can be seen that acceptable agreement is achieved – the observed deformation is less than 5% for all cases considered in the experiment. Thus, droplet deformation can be negligible in the velocity regime considered in the present work, and its effect on the flow drag coefficient can be neglected. Large deformation is observed experimentally at high air velocity, however, it is extremely challenging to quantify this due to the hysteresis of contact angle as mentioned previously.

5.2. Detachment velocity

The analytical results of the detachment velocity using the new correlation for the drag coefficient (Eqs. (1) and (2)) are compared to various experimental data as presented in Fig. 9. Because the drag coefficient in the entrance region varies with the distance from the inlet, we skip the analytical solution for that in the entrance region. In Fig. 9, the experimental data is compared with analytical solution for $1.0 \text{ mm} \times 1.6 \text{ mm}$ channel with hydrophobic carbon paper (wet proofed with 30 wt% PTFE loading). The contact-angle hysteresis is set as 40° in the analytical solution. The operating condition is 1 atm and 25°C . It shows a good agreement with the new correlation of the drag coefficient for the fully developed region. In the experiment, the detachment velocity for droplets in the entrance length is higher than that in fully developed condition, which is consistent with the force-balance analysis in [14]. Note that the droplets considered experimentally are relatively large with diameter over 0.5 mm .

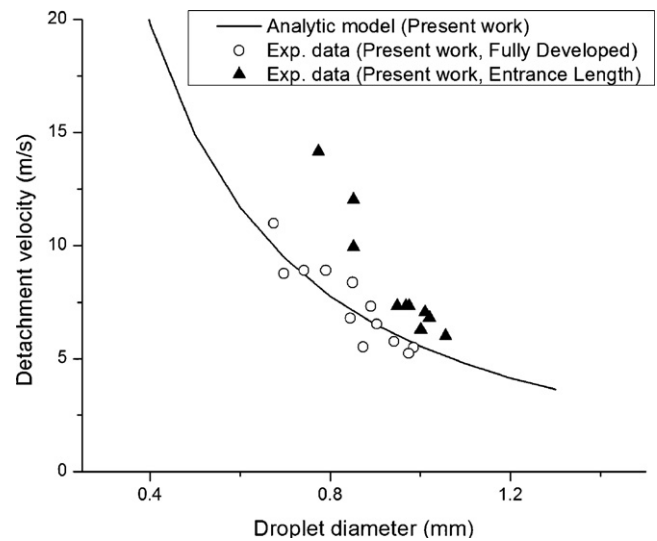


Fig. 9. The detachment velocities at the fully developed and entrance regions.

From the analytical solution, a $Re-We$ correlation was developed at the detachment velocity [14], which is plotted in Fig. 10 in comparison with the experimental data. The $Re-We$ relation based on new correlation of the drag coefficient (i.e. Eq. (2)) is shown for various H/r values. For the comparison, H/r values of several points are indicated in the figure. The ratio between droplet radius and channel height (H/r) of experimental data ranges from 1.9 to 2.9. The experimental Weber numbers show good agreement with the analytical solution.

The analytical solution is also compared to other experimental work in larger channel dimension ($7.0 \text{ mm} \times 2.7 \text{ mm}$) with similar GDL materials (hydrophobic carbon paper & cloth) [9]. The average static contact angle in the experiment is 130° for carbon paper and 145° for carbon cloth [9,18]. In Fig. 11, the experimental data is compared with analytical results. The present analytical model shows acceptable agreement with experimental data. In this study, the carbon paper has a higher detachment velocity than the carbon cloth and the analytical model also follows the same trend. As expected, the detachment velocity decreases as droplet diameter increases.

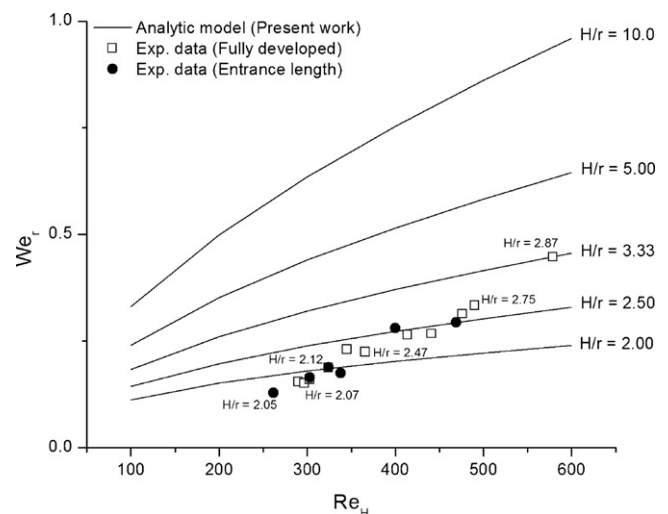


Fig. 10. Comparison of the Weber number between the experiment data and analytic solutions.

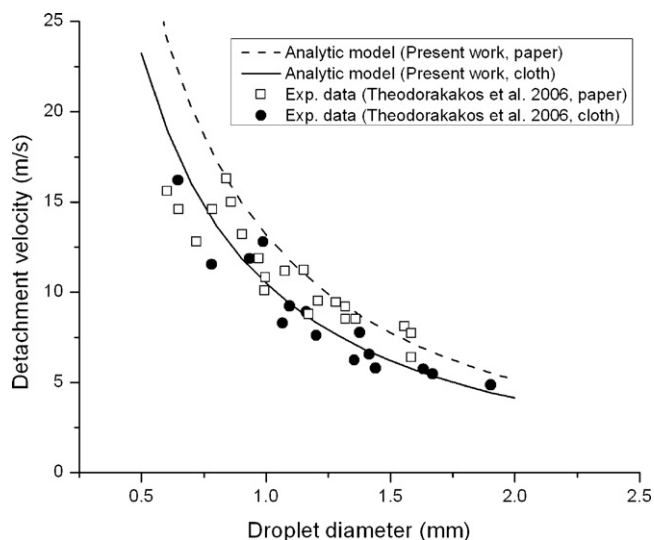


Fig. 11. Comparison of the detachment velocity between analytic solutions and experimental data [9].

Further, in PEFCs various reactants and flow conditions are encountered, such as different temperatures and reactants (hydrogen, air, and reformat). For example, PEFCs usually work in a range of temperature such as between 20 and 80 °C. The surface tension will change from around 0.0728 N m⁻¹ at 20 °C to 0.0626 N m⁻¹ at 80 °C, about 15% difference. Gas composition changes with temperature as well. The analytical solution, however, can apply to those conditions and different gases by considering the corresponding properties such as surface tension and gas density. For example, the change in the detachment velocity between 20 and 80 °C can be directly evaluated using Eq. (2).

Again, understanding the detachment velocity as a function of material properties, channel dimension, and operating condition is important to optimize the GDL surface properties, water management, and control strategy. Droplets on GDL surfaces cause liquid accumulation and can block channel flows when several droplets merge. By choosing proper material properties (e.g. contact angle, see the Weber number) and channel dimension using the analytical solution, the detachment velocity can be reduced and droplet effect can be diminished.

6. Conclusion

In the present work, the analytical solutions (obtained by approximating the water droplet shape as spherical) for droplet deformation and detachment in micro gas flow channels were compared with the VOF numerical simulation and experimental data. We used both the VOF and experimental visualization to evaluate the dynamics of droplet deformation. The pressure distributions around liquid water droplet computed numerically indicates a high pressure near the stagnation point and low pressure at the site where the air flow accelerates. The pressure difference changes the curvature of droplets, but the droplet deformation is small at relatively low velocities (<2 m s⁻¹). Quantitative comparisons between the analytical solution and experiment/numerical results show reasonably good agreement. Detachment velocity measured experimentally is also compared with the analytical solution – acceptable agreement with experimental data for various channel geometries is achieved. Lastly, the *We*–*Re* correlation at detachment velocity derived from the analytical solution was also compared to the experimental data, indicative of good agreement in the range of *H/r* values considered in the present work. The fundamental knowledge obtained in the present work is important to the understanding of the droplet dynamics in the gas flow channels of PEFCs and the optimization of GDL/channel design and operating conditions.

References

- [1] Y. Wang, K.S. Chen, J. Mishler, S.C. Cho, X.C. Adroher, *Appl. Energy* 88 (2011) 981–1007.
- [2] C.Y. Wang, *Chem. Rev.* 104 (2004) 4727–4765.
- [3] K. Jiao, X. Li, *Prog. Energy Combust. Sci.* 37 (3) (2011) 221–291.
- [4] X.G. Yang, F.Y. Zhang, A.L. Lubawy, C.Y. Wang, *Electrochem. Solid State Lett.* 7 (2004) A408–A411.
- [5] Y. Wang, S. Basu, C.Y. Wang, *J. Power Sources* 179 (2008) 603–617.
- [6] K.S. Chen, M.A. Hickner, D.R. Noble, *Int. J. Energy Res.* 29 (2005) 1113–1132.
- [7] H.P. Ma, H.M. Zhang, J. Hu, Y.H. Cai, B.L. Yi, *J. Power Sources* 162 (2006) 469–473.
- [8] Y. Wang, *J. Electrochem. Soc.* 156 (10) (2009) B1134–B1141.
- [9] A. Theodorakakos, T. Ous, M. Gavaises, J.M. Nouri, N. Nikolopoulos, H. Yanagihara, *J. Colloid Interface Sci.* 300 (2006) 673–687.
- [10] X. Zhu, Q. Liao, P.C. Sui, N. Djilali, *J. Power Sources* 195 (2010) 801–812.
- [11] A. Bazylak, D. Sinton, N. Djilali, *J. Power Sources* 176 (2008) 240–246.
- [12] L. Hao, P. Cheng, *Int. J. Heat Mass Transfer* 53 (5–6) (2010) 1243–1246.
- [13] E.C. Kumbur, K.V. Sharp, M.M. Mench, *J. Power Sources* 161 (2006) 333–345.
- [14] S.C. Cho, Y. Wang, K.S. Chen, *J. Power Sources* 206 (2012) 119–128.
- [15] X.C. Adroher, Y. Wang, *J. Power Sources* 196 (2011) 9544–9955.
- [16] X. Zhu, P.C. Sui, N. Djilali, *J. Power Sources* 172 (2007) 287–295.
- [17] J.U. Brackbill, D.B. Kothe, C. Zemach, *J. Comput. Phys.* 100 (1992) 335–354.
- [18] K.S. Chen, Sixth International Conference on Fuel Cell Science Engineering and Technology, Denver, Colorado, FUELCELL2008-65137, 2008.